Int. J. Electrochem. Sci., 9 **(2014)** 5803 - 5811

International Journal of
ELECTROCHEMICAL
SCIENCE
www.electrochemsci.org

Short Communication

Effects of Hydrogen on Stress Corrosion Cracking Behavior of Ultra-High Strength Steel 23Co14Ni12Cr3Mo

Chen WEN, Mei YU, Songmei LI, Xiangcheng LI, Jianhua LIU[*]

School of Materials Science and Engineering, Beihang University, Beijing, 100191, China
[*]E-mail: liujh@buaa.edu.cn

Received: 9 May 2014 / *Accepted:* 6 June 2014 / *Published:* 16 July 2014

Susceptibility of 23Co14Ni12Cr3Mo ultra-high strength steel to stress corrosion cracking (SCC) in a 3.5% NaCl solution was studied with different hydrogen charging specimens by using slow strain rate tests (SSRT), constant load tests (CL) and electrochemical evaluations. The fracture morphologies were characterized by SEM and optical cameras. It is shown that as hydrogen charging time (T_h) increases from 0h to 72h, the yield strength decreases from 1606MPa to 957MPa, and failure time (T_f) from 1.65×10^5s to 9.91×10^4s by SSRT. T_f decreases from 57h to 43h with increasing T_h by CL. Compared the specimen of 72h with that of 0h, the fracture surface of 72h shows a bigger transgranular fracture region by SSRT, and a toughness transgranular fracture for the specimen of 0 h. While brittle fractures with micro porous morphology for that of 72h by CL, which indicates that hydrogen improve the brittleness of 23Co14Ni12Cr3Mo steel. The effects of hydrogen on stress corrosion cracking and electrochemical behaviors were discussed by hydrogen defects.

Keywords: 23Co14Ni12Cr3Mo, ultra-high strength steel, Hydrogen embrittlement, constant load, slow strain rate test

1. INTRODUCTION

Stress corrosion is one of the most serious limitations for the use of ultra-high strength steels on engineering applications [1, 2]. SSRT and CL tests are widely used on SCC research as the basic experimental technique to promote the incidence of cracking and to determine the ranking of susceptibility of ultrahigh strength steels in several corrosive environments[3, 4]. CL is the most widely used method to study SCC process of materials due to its relatively simple experimental procedures [5~7]. However, it is hard to achieve steady state in the CL test on the measured properties as the stress exponents are extracted from the linear portion at the rear end of the holding segment [4]. The SSRT method is a useful technique to complement the CL test method in pointing to the influence

of some metallurgical parameters and to differentiate more accurately the behavior of steels [8]. It is widely used to evaluate hydrogen embrittlement and susceptibility to SCC of steels [9~12].

With the use of 23Co14Ni12Cr3Mo steel of ever-increasing strength lever, the steel must meet stringent requirements in fracture toughness and resistance to hydrogen embrittlement (HE) [13, 14]. In order to identify the influence of hydrogen on SCC behavior of 23Co14Ni12Cr3Mo steel, many researchers have made efferts on the diffusivity of hydrogen into the steel [14, 15] and the state of hydrogen in the steel [16, 17], which suggested that hydrogen formed traps and led to internal HE.

Previous studies on SCC of 23Co14Ni12Cr3Mo steel have assumed that the change of SCC susceptibility with strain rate can be divided into three regions as stress-dominated region, SCC-dominated region, and corrosion-dominated region, respectively[18, 19]. In this work, the effects of hydrogen on SCC of 23Co14Ni12Cr3Mo ultra-high strength steel in a 3.5% NaCl solution were investigated by using SSRT and CL tests, and the mechanism of hydrogen effects were discussed.

2. EXPERIMENTAL

2.1 Material and heat treatment

Small specimens of 23Co14Ni12Cr3Mo were cut from a forged and annealed bar, which was heat treated as follows: solution treated in vacuum at 885°C vacuum for 1h, air cooled to room temperature for 2h, chilled at -73°C for 1h, and tempered at 482 °C for 5h. The chemical composition is given in table1. The σ_b and $\sigma_{0.2}$ of the material resulting from this heat treatment are 1960 MPa and 1690 MPa, respectively. The microstructure of the steel mainly consists of lath/plant martensite with few reverted austenite, which was shown in Fig.1.

Table 1. Nominal composition of ultra-high strength steel 23Co14Ni12Cr3Mo,wt%

Material	C	Co	Ni	Cr	Mo	Fe
23Co14Ni12Cr3Mo	0.23	13.4	11.1	3.1	1.2	Bal.

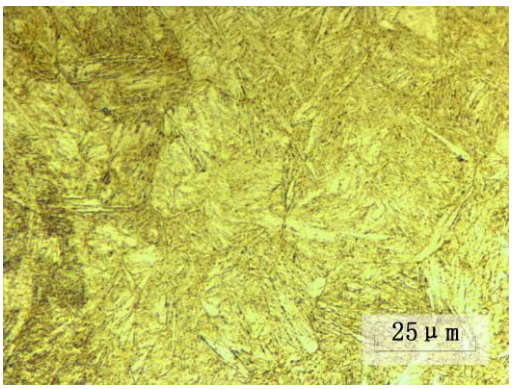

Figure 1. Microstructure of 23Co14Ni12Cr3Mo Steel

2.2 Electrochemical Hydrogen charging

Hydrogen was charged into specimens that were maintained current statically at a constant value in 0.1mol/L NaOH solution at ambient temperature for 24h, 48h, 72h, and 96h. The hydrogen content was determined immediately after electrochemical charging by RH600 Hydrogen Determinator. The hydrogen detected contents were mentioned by our previous work [20].

2.3 Stress corrosion tests

The forged bar was cut into plate specimens (gauge size: 40×5×1.5mm) in tensile direction for tensile tests. The specimens were grinded to 500 grades and electrochemical charged for 24h, 48h, 72h, which were prepared for stress corrosion tests. The SSR tests were carried out in 3.5wt%NaCl solution by using Letry SSRT Machine (WDML-5) with strain rate of 10^{-6}, and CL tests were loaded at a constant load (80% $\sigma_{0.2}$) by Letry CL Machine (TJRSS60). After tests, the fracture surfaces were characterized by scanning electron microscope (SEM3400). Relative elongation percentage and contraction of area were calculated by equation (1) as followed [21].

$$R = \frac{\lambda_t - \lambda_0}{\lambda_0} \times 100\% \quad \text{..... (1)}$$

Where R is elongation percentage and contraction of area, λ_t and λ_0 are extension amount or extraction amount at failure time t and 0.

2.4 Electrochemical measurements

The electrochemical measurements were performed by using a conventional three-electrode electrochemical cell on a princeton 2273 electrochemical system with a specimen of 23Co14Ni12Cr3Mo steel of 1 cm in diameter as working electrode. Large platinum acted as the counter electrode. A saturated calomel electrode (SCE) was used and all potentials were referred to this electrode. All electrochemical experiments were performed in a 3.5 wt% NaCl solution at room temperature.

3. RESULTS AND DISCUSSIONS

3.1 Stress corrosion results

The curves of stress to time of 23Co14Ni12Cr3Mo steel and related elongation and reduction in area by SSRT are shown in Fig.1 (a) and Fig.1 (b), respectively. As T_h increases from 0h to 72h, the yield strength decreases from 1606MPa to 957MPa and T_f from 1.65×10^5s to 9.91×10^4s. The elongation and reduction in area of the specimen decrease with T_h. It's indicated that hydrogen increases the embrittlement and leads to quicker failure.

Fig.2 shows the plots of T_f to T_h by CL at 80%$\sigma_{0.2}$ of 23Co14Ni12Cr3Mo steel and related elongation and reduction in area. T_f decreases from 57h to 43h with increasing T_h. Elongation and reduction in area of the specimen shows the same trend with the results by SSRT.

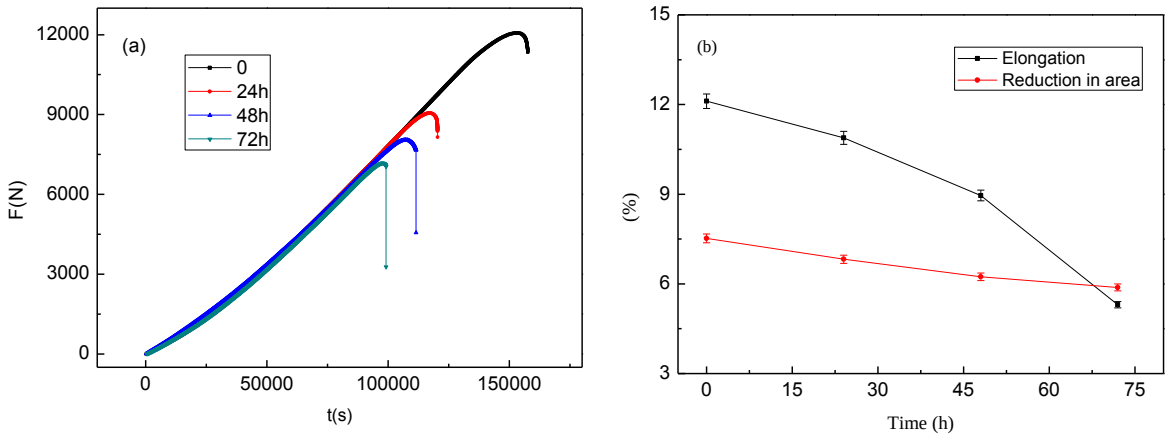

Figure 1. The curves of stress to time by SSRT of 23Co14Ni12Cr3Mo Steel

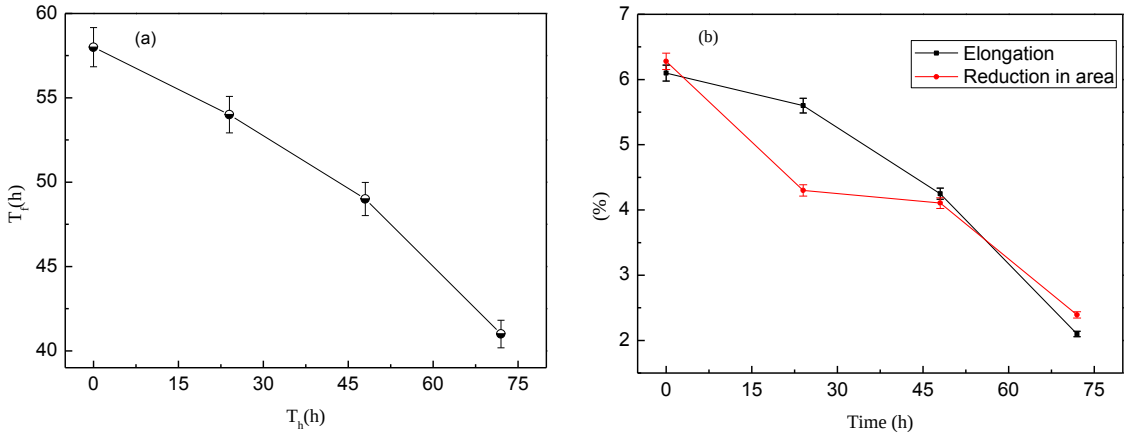

Figure 2. Plots of T_f to T_h by CL at 80%$\sigma_{0.2}$ of 23Co14Ni12Cr3Mo Steel

3.2 Fracture morphologies

The fracture morphologies by SSRT of 23Co14Ni12Cr3Mo steel with and without hydrogen charging are shown in Fig.3. Fracture morphologies with T_h for 0h and 72h have two small regions. Fig.3(a)~3(d) present a higher magnification view of the fractographies of the specimen. The fracture surface morphology in Region (a) comprises transgranular fracture. Fig3(b) shows that the appearance is brittle, with some second cracks. In contrast, the fracture surface with T_h for 72h shows a bigger transgranular fracture region (Fig.3(d)) compared with that for 0h.The region in Fig.3(c) presents an environment-induced cracking surface, which includes micro porous morphology of hydrogen defects. The effect of hydrogen porous promotes the failure and reduces the toughness of the steel.

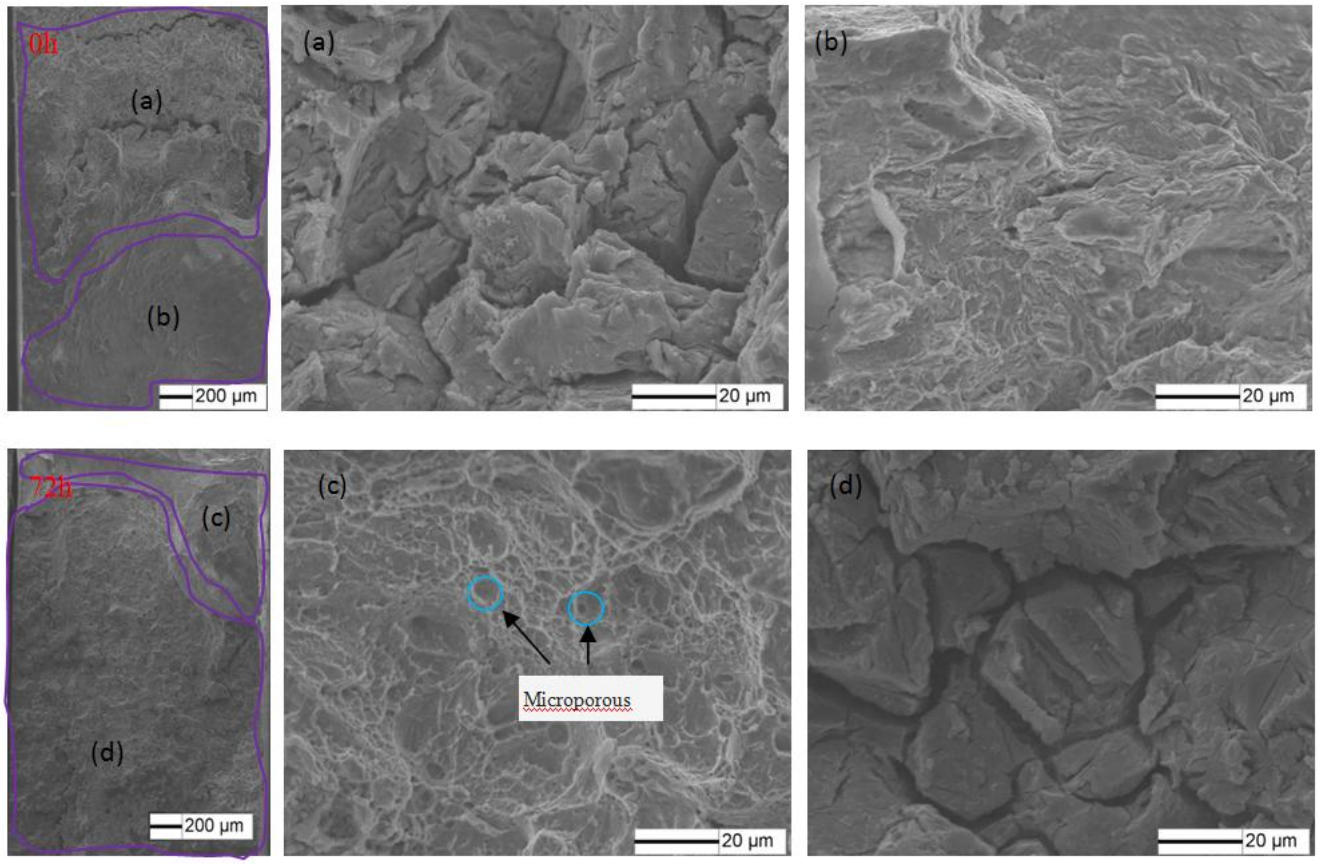

Figure 3. Fracture morphologies of specimens by SSRT of 23Co14Ni12Cr3Mo Steel: (a)~(d) present a higher magnification view of the fractographies of the specimen.

Fig.4 shows the fracture morphologies by CL of 23Co14Ni12Cr3Mo steel with T_h for 0h and 72h. The fracture surface of specimens tested of 0h shows significant ductility, higher than that of 72h, which is consistent with the results in Fig.2. It is shown a toughness transgranular fracture for the specimen of 0 h, while brittle fractures with micro porous morphology for that of 72h. It is indicated that hydrogen has entered the material and forms many porous defects. The defects limit the deformation of the grain and improve the brittleness of the steel.

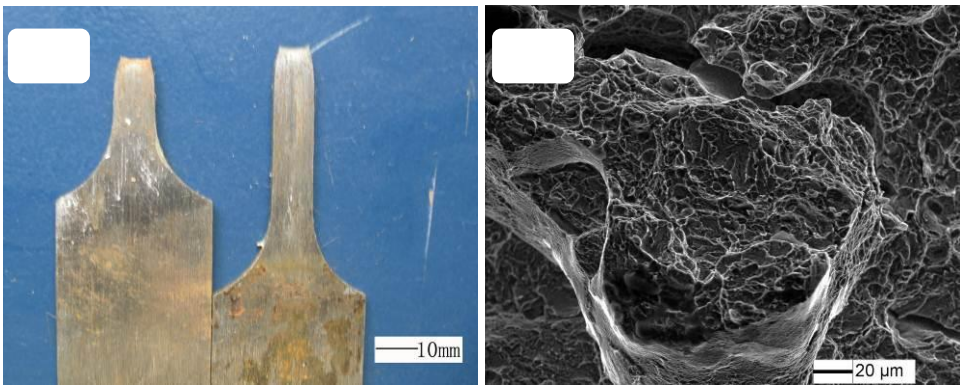

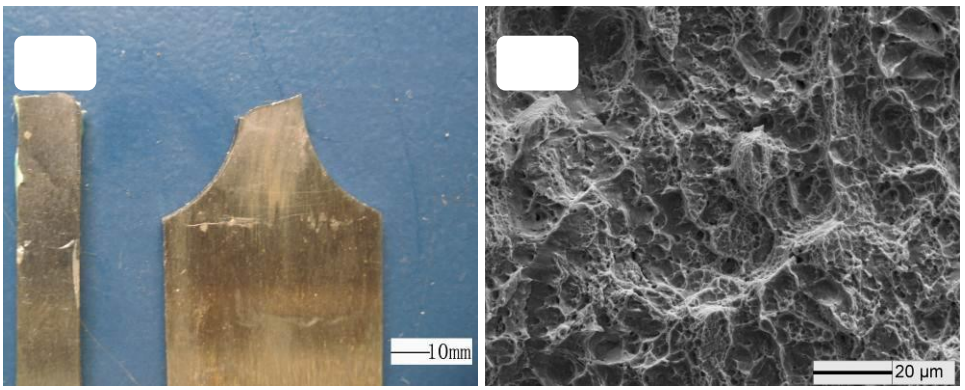

Figure 4. Fracture morphologies of specimens by CL of 23Co14Ni12Cr3Mo Steel: (a), (b) are digital and SEM views of 0h, and (c), (d) are digital and SEM views of 72h.

3.3 Electrochemical results

3.3.1 EIS results

The effects of hydrogen on the EIS behaviors were tested. The results of Nyquist plot with different hydrogen contents and related electrochemical equivalent circuits are shown in Fig.5. Where, R_l refers to the solution resistance, Q_r, R_r refers to processes occurring at the corrosion product layer /metal interface, Q_f refers to the constant phase element of the corrosion product layer and R_f refer to the resistance of the corrosion product layer. The EIS data simulated by the circuits was fitted and the summary of the results for different time is presented in Table 2. It can be obtained that it has the same circuit for different T_h, so hydrogen has little effect on the corrosion mode of 23Co14Ni12Cr3Mo steel. From the results of n_2, hydrogen changes the structure of corrosion product layer. When the hydrogen charging time reaches to 72h, n_2 is 1, which represents a pure capacitive. Hydrogen reduces the corrosion resistance of the metal from 2266 to 774Ω•cm^2. Hydrogen entering the steel forms traps [16], which activates the metal sensitive to SCC and inactivates the corrosion products. The result is agreed with the SCC results.

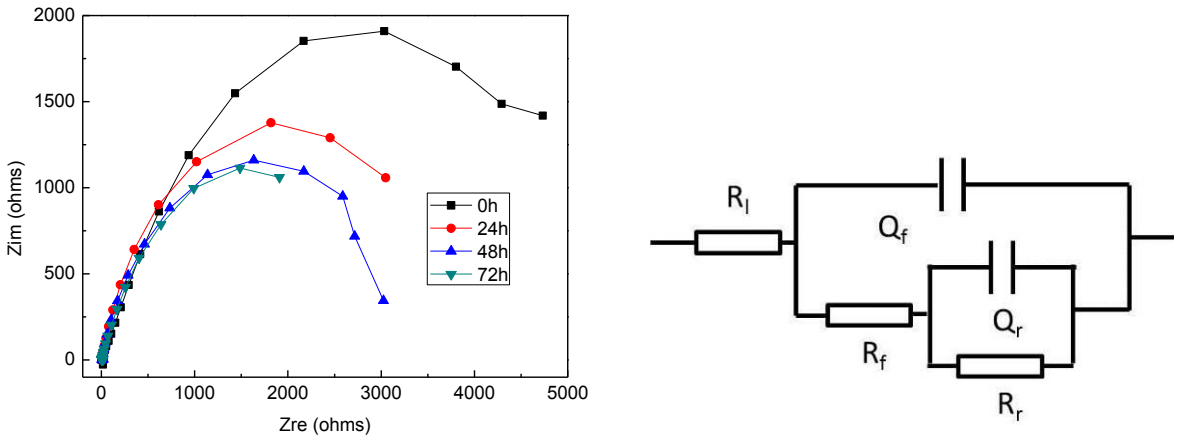

Figure 5. EIS plots of 23Co14Ni12Cr3Mo steel with different T_h

Table 2. Values of parameters calculated from Nyquist diagrams

	$R_l(\Omega)$	$Q_f(\mu F \cdot cm^{-2})$	n_1	$R_f(\Omega \cdot cm^2)$	$Q_r(\mu F \cdot cm^{-2})$	n_2	$R_r(\Omega \cdot cm^2)$
0h	4.818	1.717×10^{-4}	0.864	1160	5.469×10^{-4}	0.563	2266
24h	4.462	1.658×10^{-4}	0.777	3522	3.732×10^{-4}	0.806	1563
48h	7.507	2.621×10^{-4}	0.808	3241	4.47×10^{-5}	0.928	953
72h	4.558	6.620×10^{-4}	0.843	3269	1.058×10^{-4}	1.000	774

3.3.2 Polarization results

Fig.8 shows the polarization curves of 23Co14Ni12Cr3Mo steel in 3.5wt% with different T_h. The parameters from polarization curves are listed in Table 3. The corrosion potentials E_{corr} and the corrosion current i_{corr} of the specimens increase with the increasing T_h. Because of hydrogen traps, cathodic process resistance increases, while anodic resistance reduces with the increasing T_h. It is indicated that hydrogen accelerates the corrosion process of 23Co14Ni12Cr3Mo steel. From the results of SCC and electrochemical tests, hydrogen enters the steel, but some hydrogen in the steels that is not easy to diffuse during exposure at room temperature [22], which is presumably trapped by M_2C carbides in steel 23Co14Ni12Cr3Mo. However, tensile stress can improve hydrogen permeation, which promotes hydrogen ingress minimizing their mechanical properties to delayed fracture and accelerates corrosion of metal to a quicker failure [23~25].

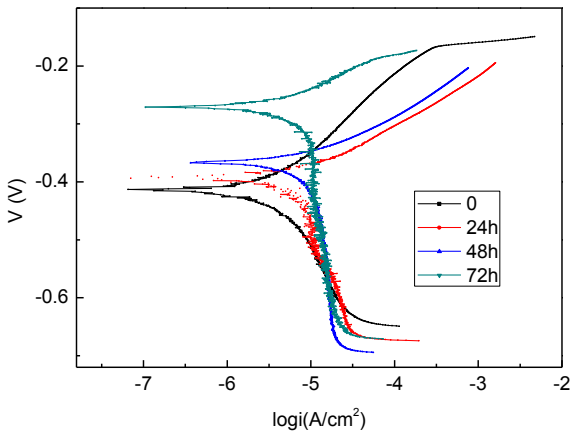

Figure 6. Polarization curves of 23Co14Ni12Cr3Mo steel with different T_h

Table 3. Values of parameters calculated from polarization diagrams

	$E_{corr}(V)$	$I_{corr}(A.cm^{-2})$	$b_a(V)$	$b_k(V)$
0h	-0.413	2.61×10^{-6}	0.1202	-0.258
24h	-0.394	6.63×10^{-6}	0.0785	-0.637
48h	-0.367	1.01×10^{-5}	0.0670	-1.107
72h	-0.271	1.03×10^{-5}	0.0657	-1.135

4. CONCLUSIONS

The SCC behavior of 23Co14Ni12Cr3Mo ultra-high strength steel with different T_h in 3.5% NaCl solution was studied. The main conclusions are summarized as follows:

1) As T_h increases from 0h to 72h, the yield strength decreases from 1606MPa to 957MPa and T_f from 1.65×10^5s to 9.91×10^4s by SSRT. T_f decreases from 57h to 43h with increasing T_h by CL.

2) The fracture surface of 72h shows a bigger transgranular fracture region by SSRT and a toughness transgranular fracture for the specimen of 0 h, while brittle fractures with micro porous morphology for that of 72h by CL, which indicates that hydrogen improves the brittleness of 23Co14Ni12Cr3Mo steel.

3) Hydrogen reduces the corrosion resistance of the metal from 2266 to 774Ω•cm^2. The corrosion potentials E_{corr} and the corrosion current i_{corr} of the specimens increase with the increasing T_h.

4) Hydrogen has entered the material and forms many porous defects. The defects limit the deformation of the grain and improve the brittleness of the steel, which activates the metal sensitive to SCC and inactivates the corrosion products.

ACKNOWLEDGEMENT
This work was supported by the National Science Foundation of China (Grant No.51171011).

References

1. R. Kerr, F. Solana, Bernstein, A.W. Thompson. *J Alloy Compd*. 6(1987)1011
2. M. Khalissi, R.K. Singh Raman, S. Khoddam. *Proc Eng.* 10(2011)3381
3. H.S. Costa-Mattos, I.N. Bastos, J.A. Gomes. *Corros. Sci.* 50(2008)2858
4. E. Akiyama, K. Matsukado, S.J. Li, K. Tsuzaki. *Appl. Surf Sci*. 257(2011)8275
5. S. Lu, C.D.C. Wun, L.F. Yong, C. Zhong. *Mater. Sci. Eng. A*. 532(2012)505
6. B. Mathias, R. Stefan, S. Hans-Peter, S. Thomas, V. Sannakaisa.*Corros. Sci*. 63(2012)129
7. J. Xu, E.H. Han, X.Q. Wu. *Corros. Sci*. 63(2012)91
8. H. Margot-Marette, G. Bardou, J.C. Charbonnier. *Corros. Sci*. 27(1987)1009
9. M.Q. Wang, E. Akiyama, T. Kaneaki. *Corros. Sci*. 49(2007)4081
10. S.J. Li, Z.G. Zhang, E. Akiyama, K. Tsuzaki, B.P. Zhang. *Corros. Sci.* 52(2010)1660
11. M. Castellote, J. Fullea, P.G. de Viedm, C. Andrade, C. Alonso, I. Llorente, X. Turrillas, J. Campob, J.S. Schweitzerc, T. Spillanec, R.A. Livingstond, C. Rolfse, H.W. Becker. *Nucl. Instrum. Meth. Phys. Res. Sect. B: Beam Interact. Mater. Atom.* 259(2007)975
12. A. Contreras, A. Albiter, M. Salazar, R. Perez. *Mater. Sci. Eng*. 25(2005)45
13. N. Eliaz, A. Shachar, B. Tal, D. Eliezer. *Eng. Fail. Analys*. 9(2002)167
14. D. Figueroa, Robinson. *Corros. Sci.* 52(2010)1593
15. P.A. Sundaram, D.K. Marble. *J. Alloy. Comp*. 360(2003)90
16. D.M. Li, R.P. Gangloff, J.R. Scully. *Metall. Mater. Trans*. A. 35(2004)849
17. R. L.S. Thomas, J. R. Scully, R.P. Gangloff. *Metall. Mater. Trans*. A. 34(2003)327
18. J.H. Liu, S. Tian, S.M. Li, M. Yu. *Acta Aeron. et Astron. Sin*. 32(2011)1164
19. L.F. Wu, S.M. Li, J.H. Liu, M. Yu. *J. Centr. South Univers*. 19(2012)2726
20. J.H. Liu, C. Wen, M. Yu, S.M. Li. *J. Mater. Eng. Perform.* 8(2013)1059
21. D. Figueroa, M.J. Robinson. *Corros. Sci.* 50(2008)1066

22. Y. Liu, M.Q. Wang, G.Q. Liu. *Int. J. Hydrogen Energ*. 38(2013)14364
23. A. Torres-Islas, S. Serna, B. Campillo, J. Colin, A. Molina. *Int. J. Electrochem. Sci*.7(2012)10633
24. A. Torres-Islas, S. Serna, B. Campillo, J. Colin, A. Molina. *Int. J. Electrochem. Sci*.8(2013)7608
25. Y. Liu, M.Q. Wang, G.Q. Liu. *Mater. Sci. Eng*.A.594(2014)40